CHINESE OPTICS LETTERS

Vol. 20, No. 7 | July 2022

# Optical analysis method for fast plasma characterization of high-speed miniaturized synthetic jet

Ye Yuan (袁 野)[1], Yan Zhang (张 岩)[2], Cheng Guo (郭 成)[1], Xiaolu Kang (康小录)[2], Zhong Yan (严 中)[1], Xiaoping Huang (黄小平)[1*], and Qing Zhao (赵 青)[1]

[1] School of Resources and Environment, University of Electronic Science and Technology of China, Chengdu 610054, China

[2] Shanghai Institute of Space Propulsion, Shanghai Engineering Research Center of Space Engine, Shanghai 201112, China

*Corresponding author: xphuang@uestc.edu.cn

Received February 25, 2022 | Accepted April 12, 2022 | Posted Online May 4, 2022

In this paper, a new optical analysis method for plasma characterization is proposed. Plasma characteristics are obtained directly by measuring the plasma luminous color, rather than the complex spectral diagnosis method, which is difficult to obtain at high speed. By using the light transmittance curve of the human cornea, the RGB coordinates are calculated from the measured plasma spectrum data. Plasma characteristics are diagnosed using the Boltzmann plot method and the Stark broadening method. The corresponding relationship of the electron temperature, electron density data points, and luminous color is established and analyzed. Our research results indicate that this optical analysis method is feasible and promising for fast plasma characterization.

**Keywords:** optical analysis method; plasma characteristics; spectral diagnosis; high-speed miniaturized actuator.
**DOI:** 10.3788/COL202220.073001

## 1. Introduction

The optical spectral diagnosis is widely used nowadays in plasma characterization[1–9], quality inspection[10–12], medical science[13–16], and many other fields[17–19]. The plasma diagnosis method based on the emission spectrum can be used for experimental research on the plasma characteristics of plasma synthetic jet actuators, such as electron temperature and electron density[1–9].

Narayanaswamy *et al.*[2] studied the performance of a pulsed plasma synthetic jet in supersonic flow control, measured the temperature using optical emission spectroscopy, and revealed that there is a considerable imbalance between rotation and vibration modes. Belinger *et al.*[4] studied the discharge characteristics of a plasma synthetic jet actuator powered by capacitance power supply. The temperature, volume, and duration of discharge were determined by optical measurement [optical emission spectrum and intensified charge coupled device (ICCD) photos]. Min *et al.*[20] studied the aerodynamic excitation characteristics of a nanosecond pulsed plasma synthetic jet, carried out an emission spectrum test in conventional atmospheric environment, and obtained the rotation temperature and vibration temperature. Wei *et al.*[21] studied the emission spectrum characteristics of a nanosecond pulsed synthetic jet plasma, calculated the electron temperature under various conditions by fitting the spectral lines, and obtained the variation law of electron temperature during discharge.

The above studies are based on the measured spectral data to calculate the plasma characteristic parameters such as plasma density and temperature, which is also a conventional method for spectral diagnosis of plasma. However, one disadvantage of this method is that it is difficult to realize high-speed measurement because the spectrum contains a large amount of information. To solve this problem, we propose a new optical analysis method for plasma characterization, which creatively connects the luminous color with the plasma characteristics, establishes the corresponding relationship between them, and obtains the plasma characteristics by measuring the luminous color of the plasma. Now, there are already many advanced spectrometers, such as SpectraPro HRS with the aid of ICCD and PI-MAX, which have a nanosecond time resolution. However, most of these spectrometers have a very high cost, which is at least ¥400,000. Moreover, some fast plasma experiments especially in some emergency situations should be carried out to get the plasma characteristics. A simple and auxiliary function method should be proposed to measure discharge, which can take the place of the advanced imaging spectrometers sometimes. Our method is a fast and simple method to characterize the electron temperature and electron density based on the luminous color. There are two major advantages for our method in certain conditions. First, we have a fast process for obtaining the characteristic results from the luminous image color. One can get the first-hand data quickly, especially in emergency situations.

Second, one can quickly make a rough estimation by our method if he is familiar with the luminous characteristics of plasma, which is easy for a researcher in plasma. Moreover, our method is very convenient, timely, and rapid for the application of plasma engineering. Our method provides a plasma characteristic analyzing method based on luminous color with a fast imaging record. Only three chromatic sensors are needed to record the chromatic intensities in our method. Spectral measurement uses a spectrometer to disperse incident light into a spectrum through some lenses and gratings, wherein the spectrum shines on the sensor of a linear array or area array. Usually, 2048 array sensors are used to record the light intensities to obtain 2048 pixels amplitudes. So, our method can greatly save many hardware resources, which improves the hardware running speed to increase the measurement speed.

The article is arranged as follows: the second part introduces the experimental instrument, the third part introduces the optical analysis method for plasma characterization, the fourth part is the experimental and calculation results and analysis, and the fifth part summarizes the full text.

## 2. Experimental Instruments

The discharge form in the cavity of the actuator is arc discharge in the gap between the electrodes[22]. The plasma synthetic jet actuator used for plasma characterization is shown in Fig. 1. The FX2000 optical fiber spectrometer of Shanghai Fuxiang Company was used in the diagnosis. The spectral range of FX2000 is 200–1100 nm. The highest optical resolution is 0.24 nm (FWHM). The discharge power is changed by changing the capacitance. The different working conditions selected for diagnosis are the capacitances of 0.16 μF, 0.32 μF, and 0.48 μF and the electrode spacings of 1.9 mm, 3 mm, and 4.5 mm.

## 3. Optical Analysis Method for Plasma Characterization

According to the measured spectra, we can calculate the color of light and the plasma characteristics such as electron temperature and electron density. The new optical analysis method for plasma characterization proposed by us is to first obtain the color and plasma characteristics by spectral calculation, repeat this step under different working conditions, and obtain a database of color and plasma characteristics corresponding to working conditions. After the database is established, it is no longer necessary to measure the spectra. Instead, the color information is obtained directly by taking photos, and then the plasma characteristics corresponding to the colors are directly queried in the previously established database. Because the spectrum contains a large amount of information, it is a dot matrix containing many data points, and the color is only a three-channel data point, so the color acquisition speed will be much higher than the spectrum acquisition speed, which is easier to realize high-speed measurement. Building the database is our next step for working plan. In this paper, we only demonstrate the feasibility of this method. Next, the method of calculating luminous color and plasma characteristics by the spectrum is introduced.

### 3.1. Luminous color calculation method

We use MATLAB programming to calculate the luminous color of plasma from the spectral data. The International Commission on Illumination (CIE) *XYZ* trichromatic system is generally used to characterize the color, where the color is decomposed into three primary colors: *X*, *Y*, and *Z*. The color can be uniquely determined by the coordinates of the three basic vectors *X*, *Y*, and *Z*. This color is the linear superposition of the three components *X*, *Y*, and *Z*. To calculate the coordinates of the *XYZ* system, we need to use the "light transmittance curve of human cornea," namely color matching functions (CMFs). This is the intensity portion of the unit luminous intensity received by the *X*, *Y*, and *Z* human eye sensors under different spectral wavelengths; that is, three curves with the wavelength as the abscissa axis, as shown in Fig. 2. Here, we use the CMF under CIE 1931 specification and use the interpolation function to obtain the CMF values at the wavelength points of the measured spectral data. We multiply the normalized spectral values by the CMF values of *X*, *Y*, and *Z*, respectively, and integrate them in the whole wavelength range to obtain the *X*, *Y*, and *Z* values. We

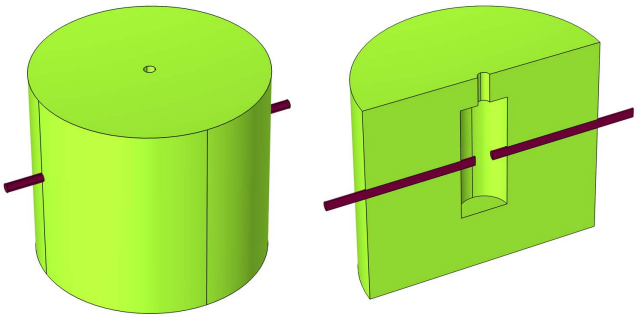

**Fig. 1.** Structure of the plasma synthetic jet actuator.

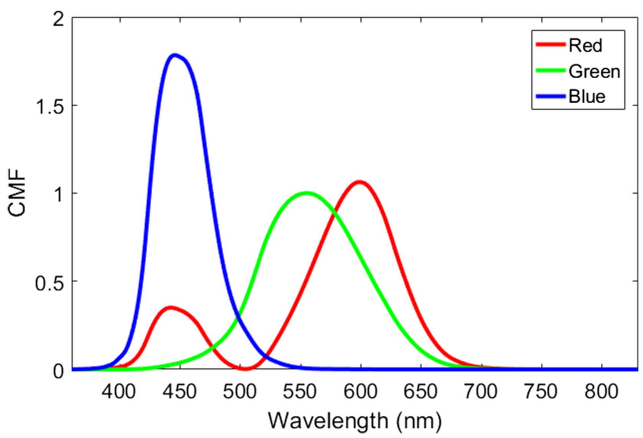


**Fig. 2.** Light transmittance curve of the human cornea.

divide these three values by $X+Y+Z$ to obtain the normalized $x$, $y$, and $z$ values. RGB is a common color system for displaying colors, so we also need to transform the coordinates of the $XYZ$ color system to the RGB coordinates system by coordinate transformation. Finally, the normalized RGB coordinates for display are obtained, and the luminous color map is made.

### 3.2. Diagnostic method for plasma characterization

Plasma electron temperature is diagnosed using the Boltzmann plot method[23].

If local thermodynamic equilibrium (LTE) is reached in the plasma, according to Boltzmann's law, the intensity $I_{mn}$ of the spectrum produced by the particle transferring from the higher energy level $m$ to the lower level $n$ is

$$I_{mn}=\frac{hcg_mA_{mn}N}{4\pi\lambda U}\exp\left(-\frac{E_m}{kT}\right), \tag{1}$$

where $h$ is the Planck constant, $c$ is the speed of light, $g_m$ is the statistical weight of the upper energy level, $A_{mn}$ is the transition probability, $N$ is the total density of particles on the upper level, $\lambda$ is the wavelength of the spectral line, $U$ is the partition function, $E_m$ is the energy of the upper level, $k$ is the Boltzmann constant, and $T$ is the excitation temperature of the electron. We take the logarithm of both sides of the equation to obtain

$$\ln\left(\frac{I_{mn}\lambda}{g_mA_{mn}}\right)=-\frac{E_m}{kT}+C. \tag{2}$$

We pick up several spectral lines of the same particle and calculate the value of $\ln(\frac{I_{mn}\lambda}{g_mA_{mn}})$. Then, we take $E_m$ as the $x$ coordinate, $\ln(\frac{I_{mn}\lambda}{g_mA_{mn}})$ as the $y$ coordinate, and plot the points. As can be seen in Eq. (2), after fitting the points to a straight line, from the slope of the line, we can obtain the temperature $T$.

The plasma electron density is diagnosed using the Stark broadening method[9]. The spectrum of $H_\alpha$ at 656.3 nm is often used in the Stark broadening method. The shape of $H_\alpha$ is named the Voigt shape, which is produced by the convolution of the Gaussian shape and the Lorentzian shape. The broadening of a Voigt shape can be expressed as

$$\Delta\lambda_V=\left[\left(\frac{\Delta\lambda_L}{2}\right)^2+\Delta\lambda_G^2\right]^{0.5}+\Delta\lambda_L, \tag{3}$$

where $\Delta\lambda_V$ is the broadening of a Voigt shape, $\Delta\lambda_L$ is the broadening of a Lorentzian shape, and $\Delta\lambda_G$ is the broadening of a Gaussian shape.

The broadening of a Gaussian shape can be expressed as

$$\Delta\lambda_G=(\Delta\lambda_I^2+\Delta\lambda_D^2)^{0.5}, \tag{4}$$

where $\Delta\lambda_I$ is the instrument broadening, and $\Delta\lambda_D$ is the Doppler broadening, which can be expressed as Eq. (5) for the $H_\alpha$ spectrum:

$$\Delta\lambda_D=4.7\times10^{-4}T_g^{0.5}, \tag{5}$$

where $T_g$ is the temperature of the gas, which is equal to the temperature of the electron in the plasma in the LTE state.

The broadening of a Lorentzian shape can be expressed as

$$\Delta\lambda_L=\Delta\lambda_S+\Delta\lambda_{\text{van}}, \tag{6}$$

where $\Delta\lambda_S$ is the Stark broadening, and $\Delta\lambda_{\text{van}}$ is the van der Waals broadening, which can be expressed as Eq. (7) for the $H_\alpha$ spectrum:

$$\Delta\lambda_{\text{van}}=5.12/T_g^{0.7}. \tag{7}$$

After we obtained $\Delta\lambda_S$, the density of electron can be expressed as Eq. (8) using the Stark broadening of the $H_\alpha$ spectrum:

$$n_e=\left(\frac{\Delta\lambda_S}{3.19}\right)^{1.723}\times10^{18}, \tag{8}$$

where $n_e$ is in $\text{cm}^{-3}$, and all the above broadenings are in nanometers (nm).

## 4. Results and Analysis

The plasma emission spectra in the visible range with different capacitances at the electrode spacing of 1.9 mm are obtained, as shown in Fig. 3. The plasma emission spectra with capacitance of 0.16 μF at different electrode spacings are shown in Fig. 4. It can be seen from the figures that some sharp spectral lines appear in the emission spectra of plasma under different working conditions. The wavelength positions of sharp lines in these six figures almost stay the same. However, there are some different sharp lines absent in different working conditions.

The plasma luminous color, electron temperature, and electron density under different working conditions are calculated and shown in Fig. 5. The normalized red, green, and blue components of RGB are also marked in the figure. As can be seen from Fig. 5(a), the electron temperature increases with the increase of capacitance. This is because increasing the capacitance means increasing the energy stored in the capacitor; that is, the input work of the actuator increases, so the energy deposited during discharge increases. Therefore, the heat energy released during the discharge increases, resulting in the increase of the plasma gas temperature. Due to the LTE, the electron temperature is equal to the gas temperature, so the electron temperature increases. It can also be seen from Fig. 5(a) that the electron density increases with the increase of capacitance. This is because, with the increase of capacitance, the discharge voltage is basically unchanged, so the energy obtained by a single electron when being accelerated in the electric field remains unchanged. As mentioned above, the total discharge energy increases, so the number of electrons accelerated in the electric field increases, and the number of ionization reactions and

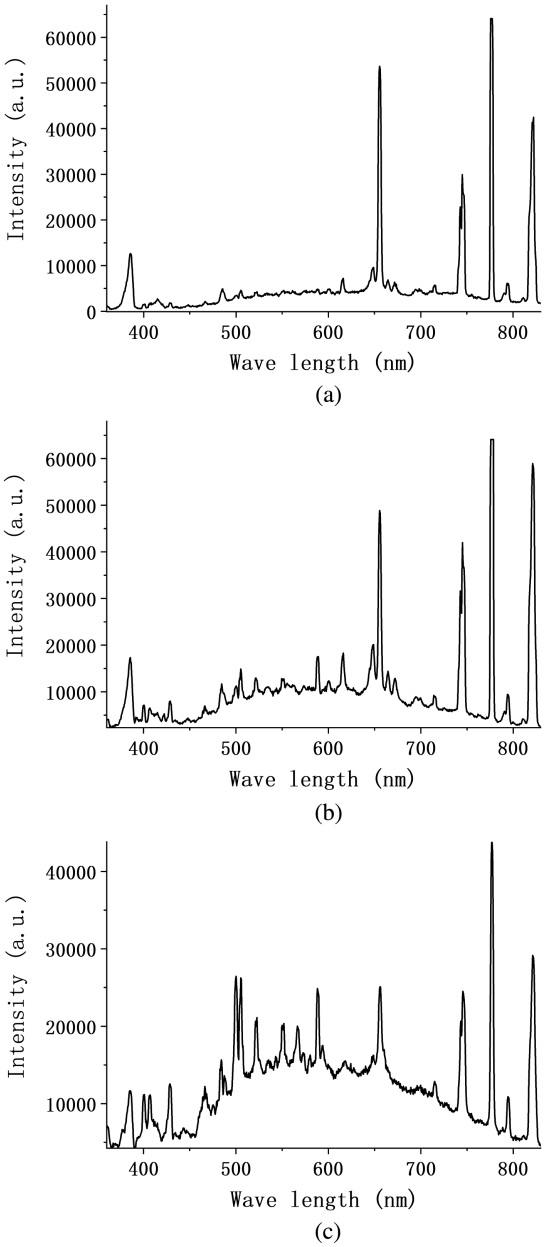


**Fig. 3.** Plasma emission spectra in the visible range with different capacitances at the electrode spacing of 1.9 mm. (a) Spectrum at 0.16 μF, (b) spectrum at 0.32 μF, and (c) spectrum at 0.48 μF.

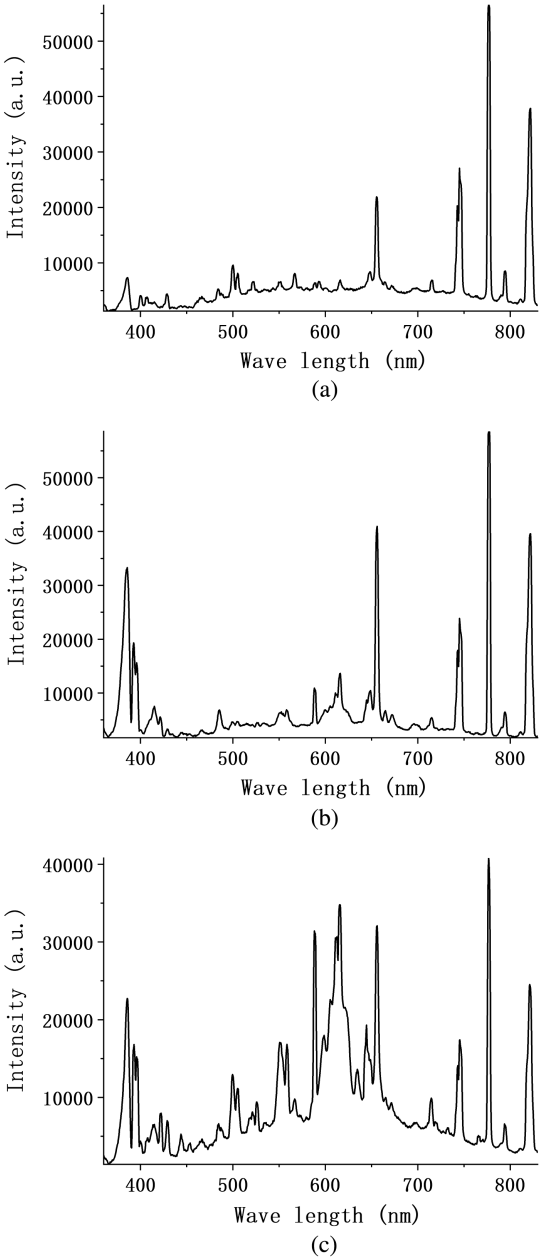


**Fig. 4.** Plasma emission spectrum in the visible range with 0.16 μF at different electrode spacings. (a) Spectrum at the electrode spacing of 1.9 mm, (b) spectrum at the electrode spacing of 3 mm, and (c) spectrum at the electrode spacing of 4.5 mm.

electron density increase. As can be seen from Fig. 5(a), under the calculated working conditions, the plasma luminescence is different light yellows. Among them, the corresponding luminous color with the plasma characteristics of electron temperature at 5344 K and electron density of $5.47 \times 10^{23}\,\mathrm{m}^{-3}$ is compared experimentally. As shown in Fig. 6, the calculated result is close to the actual color observed in the experiment. As can be seen from Fig. 5(a), with the increase of capacitance, the red component in the three primary colors first remains unchanged and then decreases, and the green and blue components increase. Because it is a normalized component, it means that the portion of red is smaller, the portions of green and blue become larger, and the portions of red, green, and blue tend to be more equal. When the portion of the three colors is equal, it shows white light, so the light emission should be closer to white light. It can be seen from the figure that the yellow of the color diagram has become lighter. With the increase of capacitance, the intensity of spectral lines mainly distributed in the region of 500–600 nm increases, and these are mainly spectral lines such as $N^+$ ions (500.515 nm, 504.510 nm, 549.567 nm, and 566.663 nm) and C atoms (587.0655 nm); that is, the content of $N^+$ ions and excited C atoms increases. In other words, the

ionization reaction intensifies, and more C atoms in the air are excited, which is consistent with the increase of electrons accelerated to high speed. The increase of spectral intensities in the region of 500–600 nm is conducive to the increase of green and blue components, because the light transmittances of green and blue are relatively large in this range. Therefore, with the increase of electron temperature and electron density, the proportions of green and blue increase.

As can be seen from Fig. 5(b), as the electrode spacing increases, the electron temperature decreases. Due to the LTE, the gas temperature decreases. The reason is as follows. First, with the increase of spacing, the air flow and heat exchange area become larger. Second, with the increase of spacing, the arc length is longer, which leads to the decrease of current density, resulting in the decrease of Joule heat released by the arc. Due to these two points, the heat generated is smaller and dissipated more, so the temperature decreases. As can be seen from Fig. 5(b), with the increase of electrode spacing, the electron density increases. This is because with the increase of electrode spacing, the discharge has more difficulty happening, the breakdown voltage increases, and the increase of spacing is faster than the increase of voltage, as a result, the electric field intensity decreases. When a single electron is accelerated in the electric field, the energy obtained by the electron is directly proportional to the electric field intensity. Therefore, the energy obtained by a single electron decreases. Meanwhile, the discharge voltage increases with the increase of electrode spacing, and thus the total discharge energy increases. Therefore, the number of electrons accelerated to high speed increases, so the number of ionization reactions increases, and the electron density increases. With the increase of electrode spacing, the proportions of green and blue decrease, and the luminous color becomes darker. This is because with the increase of capacitance, the energy gain of a single electron remains unchanged; with the increase of electrode spacing, the energy gain of a single electron decreases. The energy gain of a single electron affects the energy difference between the upper and lower energy levels of the ionization excitation reaction. The higher the energy gain is, the greater the energy difference of the reaction is, and the shorter the wavelength of the spectral line corresponding to the reaction is. Therefore, the wavelengths of the spectral lines with the larger intensity increase when the capacitance is increased are shorter than the wavelengths of the spectral lines with the larger intensity increase when the spacing is increased. This can be observed in Figs. 3 and 4. When the capacitance is increased, the spectral lines with the larger intensity increase are roughly in the range of 500–600 nm, while, when the spacing is increased, the spectral lines with the larger intensity increase are roughly in the range of 580–660 nm. The CMF of red light in the range of 580–660 nm is relatively large, so when the spacing is increased, the composition of red light increases. Because it is a relative quantity, the result is that the proportions of blue and green light decrease, and the proportion of red light increases with the decrease of electron temperature and the increase of electron density.

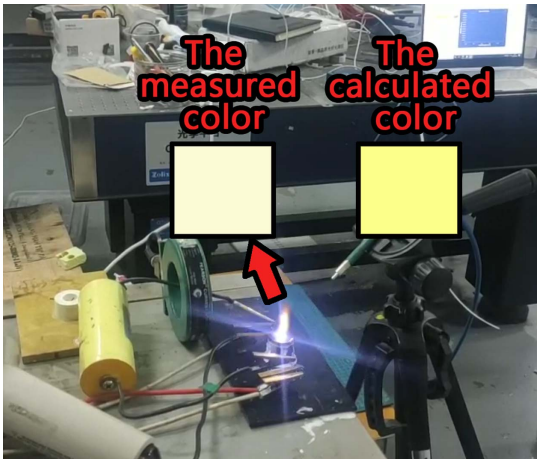


**Fig. 6.** Comparison between measured color and calculated color.

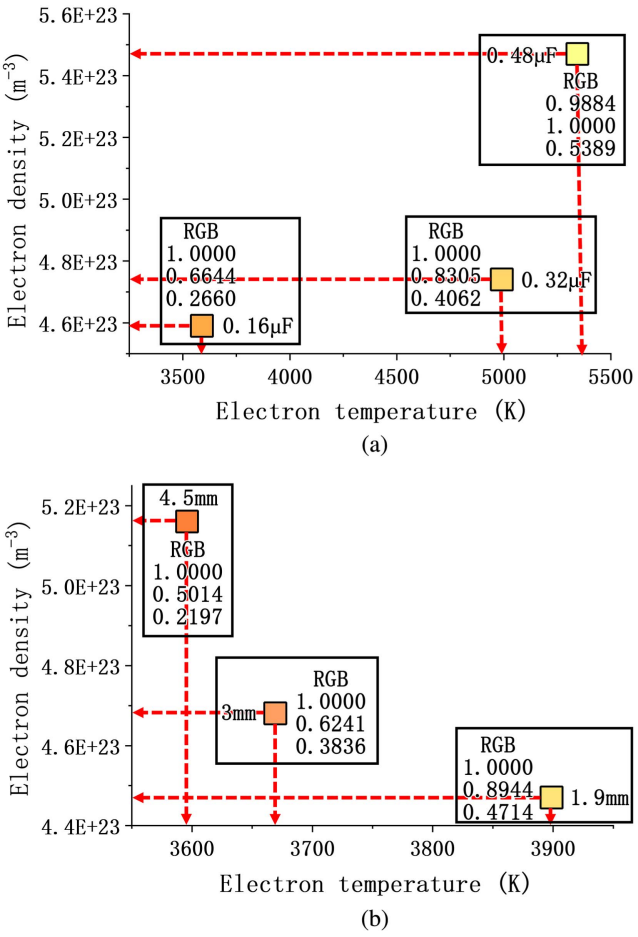


**Fig. 5.** Comparison diagram of plasma luminescence color, electron temperature, and electron density under different working conditions. (a) Comparison diagram of plasma luminescence color, electron temperature, and electron density under different capacitances at electrode spacing of 1.9 mm, and (b) comparison diagram of plasma luminescence color, electron temperature, and electron density under different electrode spacings when capacitance is 0.16 μF.

From our examples, we can see that the luminous color becomes lighter with the increase of temperature, and the changing law of luminous color with electron density is affected by different changing working conditions, which affect the coordinates of data positions in the comparison diagram of luminous color, electron temperature, and electron density. Through the above research, the corresponding relationship of electron temperature, electron density data points, and luminous color is established and analyzed. From it, we can see that the method of obtaining plasma characteristics from luminous color is feasible. After increasing the amount of data, this method can be applied, which has great advantage for realizing high-speed plasma characterization.

## 5. Conclusion

In this paper, we propose a new optical analysis method to obtain the plasma characteristics through the plasma luminous color and apply this method to the high-speed miniaturized plasma synthesis jet actuator.

With the increase of electron temperature and electron density, the proportions of green and blue increase. This is related to the increase of spectral intensities in the wavelength range of 500–600 nm caused by the increase of electrons accelerated to high speed. With the decrease of electron temperature and the increase of electron density, the proportions of blue and green light decrease, and the proportion of red light increases. This is related to the increase of spectral intensities in the wavelength range of 580–660 nm. The luminous color becomes lighter with the increase of temperature, and the changing law of luminous color with electron density is different under the influence of different working conditions, which affect the coordinates of data points in the comparison diagram of luminescence color, electron temperature, and electron density.

The method of directly obtaining plasma characteristics from luminous color is feasible. To use this method, in the early stage, we need to calculate the luminous color and plasma characteristics from the spectral data and increase the amount of data. When using this method in the later stage, we will no longer need to collect the spectra, but directly query the database by color to obtain the plasma characteristics. This method has great advantages for realizing high-speed plasma characterization.

## Acknowledgement

We thank Dr. Yan Zhou for offering the actuator and help of optical spectrum measuring experiments. This work was supported by the Key R&D Project of Sichuan Provincial Department of Science and Technology (No. 2021YFG0369), Sichuan International Science and Technology Innovation Cooperation Project (No. 2021YFH0057), National Key R&D Program of China (No. 2018YFC0603303), and State Grid Science and Technology Project (No. 5700-202127198A-0-0-00).

## References

1. J. Shin, V. Narayanaswamy, L. L. Raja, and N. T. Clemens, "Characterization of a direct-current glow discharge plasma actuator in low-pressure supersonic flow," AIAA J. **45**, 1596 (2007).
2. V. Narayanaswamy, L. L. Raja, and N. T. Clemens, "Characterization of a high-frequency pulsed-plasma jet actuator for supersonic flow control," AIAA J. **48**, 297 (2010).
3. N. Zhao, J. Li, Q. Ma, L. Guo, and Q. Zhang, "Periphery excitation of laser-induced CN fluorescence in plasma using laser-induced breakdown spectroscopy for carbon detection," Chin. Opt. Lett. **18**, 083001 (2020).
4. A. Belinger, N. Naudé, J. P. Cambronne, and D. Caruana, "Plasma synthetic jet actuator: electrical and optical analysis of the discharge," J. Phys. D **47**, 345202 (2014).
5. K. Inoue, S. Takahashi, N. Sakakibara, S. Toko, T. Ito, and K. Terashima, "Spatiotemporal optical emission spectroscopy to estimate electron density and temperature of plasmas in solution," J. Phys. D **53**, 235202 (2020).
6. C. Pan, "Diagnosis the physical characteristics of pulsed MIG welding arc by spectrum," Ph.D. Thesis (Shanghai Jiao Tong University, 2013).
7. L. Min, X. Hao-jun, W. Xiao-long, L. Hua, and S. Chen, "Experimental study of generation and spectroscopic diagnosis of inductively coupled plasma in closed cavity," J. Air Force Eng. Univ. **16**, 10 (2015).
8. L. Lei, X.-D. Chen, C.-X. Yuan, and Z.-X. Zhou, "Emission spectrum diagnose to Ar plasma jet," Chin. J. Lumin. **40**, 1049 (2019).
9. C. J. Chen, "Optical emission spectroscopic diagnosis on atmospheric-pressure pulse-modulated surface wave plasma and its characteristics," Ph.D. Thesis (Dalian University of Technology, 2019).
10. M. Zhao, D. Zhang, L. Zheng, O. Condliffe, and Y. Kang, "Rapid quantitative detection of mineral oil contamination in vegetable oil by near-infrared spectroscopy," Chin. Opt. Lett. **18**, 043001 (2020).
11. L. X. Liu, H. T. Huan, M. Andreas, and X. P. Shao, "Multiple dissolved gas analysis in transformer oil based on Fourier transform infrared photoacoustic spectroscopy," Spectrosc. Spectr. Anal. **40**, 684 (2020).
12. A. Deng, Z. Zeng, and J. Deng, "VIPA-based two-component detection for a coherent population trapping experiment," Chin. Opt. Lett. **19**, 083001 (2021).
13. J. Jo, J. Siddiqui, Y. Zhu, L. Ni, S.-R. Kothapalli, S. A. Tomlins, J. T. Wei, E. T. Keller, A. M. Udager, X. Wang, and G. Xu, "Photoacoustic spectral analysis at ultraviolet wavelengths for characterizing the Gleason grades of prostate cancer," Opt. Lett. **45**, 6042 (2020).
14. Y. W. Chu, F. Chen, Y. Tang, T. Chen, Y. X. Yu, H. L. Jin, L. B. Guo, Y. F. Lu, and X. Y. Zeng, "Diagnosis of nasopharyngeal carcinoma from serum samples using hyperspectral imaging combined with a chemometric method," Opt. Express **26**, 28661 (2018).
15. K. Chen, Y. Qin, F. Zheng, M. Sun, and D. Shi, "Diagnosis of colorectal cancer using Raman spectroscopy of laser-trapped single living epithelial cells," Opt. Lett. **31**, 2015 (2006).
16. C. Zhu, T. M. Breslin, J. Harter, and N. Ramanujam, "Model based and empirical spectral analysis for the diagnosis of breast cancer," Opt. Express **16**, 14961 (2008).
17. G. Chen, J. Zhu, and X. Li, "Influence of a dielectric decoupling layer on the local electric field and molecular spectroscopy in plasmonic nanocavities: a numerical study," Chin. Opt. Lett. **19**, 123001 (2021).
18. Y. Z. Zhao, Y. L. Su, X. Y. Hou, and M. H. Hong, "Directional sliding of water: biomimetic snake scale surfaces," Opto-Electronic Adv. **4**, 210008 (2021).
19. J. Li, J. Hu, J. Ma, X. Wen, and D. Li, "Identifying self-trapped excitons in 2D perovskites by Raman spectroscopy," Chin. Opt. Lett. **19**, 103001 (2021).
20. M. Jia, H. Liang, H. Song, P. C. Liu, and Y. Wu, "Characteristic of spark discharge plasma jet driven by nanosecond pulses," High Volt. Eng. **37**, 1493 (2011).
21. L. Wei, Z.-X. Wang, and S. Li, "Emission spectrum characteristics of nanosecond pulsed spark plasma," Adv. Electr. Electron. Eng. **35**, 29 (2016).
22. Z. Yan, "Novel plasma synthetic jet and its application in shock wave control," Ph.D. Thesis (National University of Defense Technology, 2018).
23. A. Belinger, "Plasma synthetic jet actuator: electrical and optical analysis of the discharge," J. Phys. D **47**, 345202 (2014).